Bone Chemical Composition Analysis Using Photoacoustic Technique

Ting Feng[1,2], Yejing Xie[1], Weiya Xie[2], Dean Ta[3] and Qian Cheng[2,4]*

[1]School of Electronic and Optical Engineering, Nanjing University of Science and Technology, Nanjing, China, [2]Institute of Acoustics, School of Physics Science and Engineering, Tongji University, Shanghai, China, [3]Department of Electronic Engineering, Fudan University, Shanghai, China, [4]Key Laboratory of Spine and Spinal Cord Injury Repair and Regeneration of Ministry of Education, Orthopaedic Department of Tongji Hospital, Tongji University School of Medicine, Shanghai, China

Photoacoustic (PA) signal analysis based on ultrasonic wave detection can provide both high-sensitivity optical contrast information and micro-architectural information which is highly related with the chemical composition of tissue. In this study, the feasibility assessment of bone composition assessment was investigated using the multi-wavelength PA analysis (MWPA) method which could reflect the molecular information. By illuminating a bone specimen using a laser light with wavelength over an optical spectrum ranging from 680 to 950 nm, the optical absorption spectrum of the bone was acquired. Then, with the optical absorption spectra of all optical absorption chemical components in the known bone, a spectral unmixing procedure was performed to quantitatively assess the relative content of each chemical component. The experimental results from rabbit bones show that MWPA method can be used to assess chemical components related to bone metabolism. Our study confirmed that PA technique can be used as a novel bone diagnostic technique by providing new information about the quantity of bone and identifying biomarkers of bone that can improve the current diagnostic imaging techniques.

Keywords: photoacoustic, bone assessment, chemical composition, multi-wavelength photoacoustic analysis, osteoporosis

INTRODUCTION

Osteoporosis, a serious public health threat with significant physical, psychological and economic impacts, is expected to increase in association with worldwide aging of the population. In osteoporosis, the bone mineral density (BMD) decreases, bone microarchitecture (BMA) deteriorates, and the amount and type of proteins in bone alter [1]. Currently, most clinically used non-invasive assessment methods are based on the use of X-ray or ultrasound [2, 3]. These methods, in spite of the applicability to measure bone mineral density (BMD) as well as some mechanical properties, have limited sensitivity to monitor the chemical or molecular changes in the bone. In addition, X-ray based techniques use ionizing radiation, which is not ideal for pediatric, or long-term repetitive monitoring. Quantitative ultrasound (QUS) technology as a practical, low-cost alternative has already led to clinical instrumentation [4, 5]. The QUS bone assessment method is primarily based on the measurement of sound velocity (SOS) and broadband ultrasound attenuation (BUA) through a given tissue. However, the specificity of QUS is limited when pathogenic bone diseases are determined by microstructure and chemical changes [6–8]. Bone quantity and quality are dependent on not only the mass and structure of non-organic mineral matrix but also the organic matrix which is associated with the bone blood flow and cellular metabolism. Recently, it has been

FIGURE 1 | (A,B) The schematic diagram of the experiment setup. **(C)** The photograph of the bone sample. **(D)** An example of the PA signal generated by the bone specimen. **(E)** An example of the power spectrum density (PSD) of the PA signal generated by the bone.
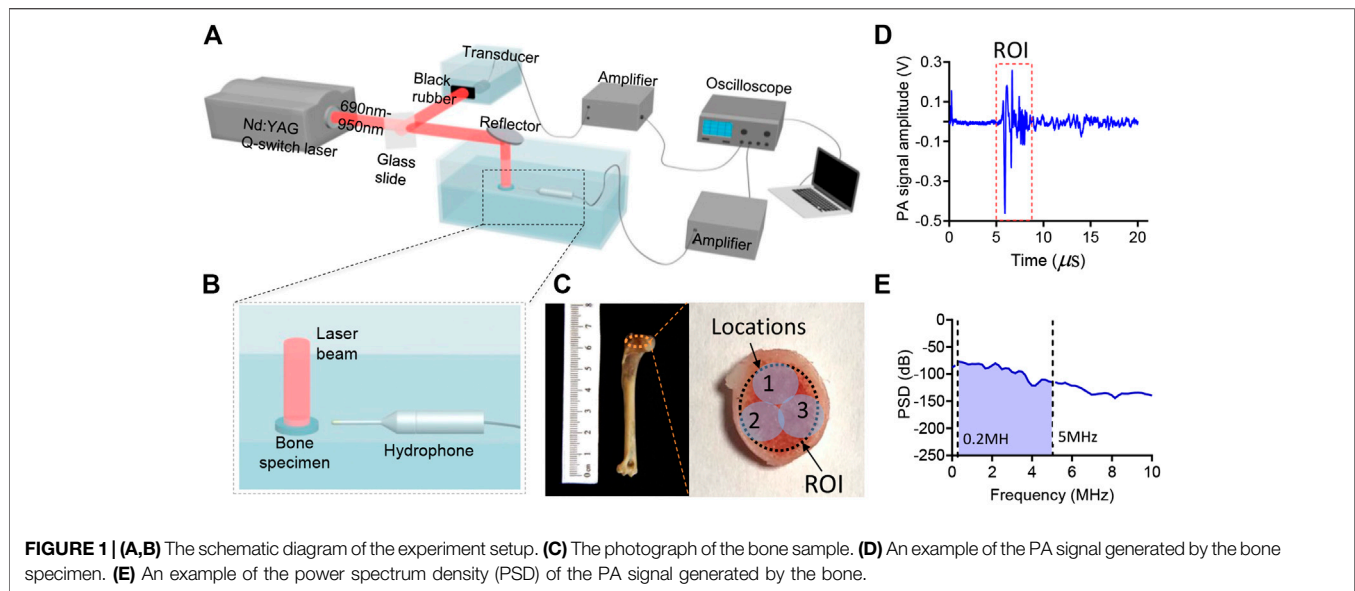
reported that magnetic resonance imaging (MRI) can distinguish changes in bone marrow lipid content and bone microarchitecture between normal bone and osteopenia bone [9–11]. Due to the high cost and complexity, MRI examinations are impossible to replace standard DEXA (Dual-Energy X-ray Absorptiometry) measurements with more advanced MRI analysis. In prior studies, optical spectroscopic techniques have been used to evaluate how the alterations of bone composition contribute to bone quality changes related to aging, disease, or injury [12–18]. However, traditional optical techniques suffer from limited spatial resolution and the overwhelming optical scattering in biological tissues, thus reducing the efficacy of skeletal imaging *in vivo*.

The emerging biomedical photoacoustic (PA) techniques have a unique ability to probe the highly sensitive optical absorption contrast in deep biological tissues [19–23]. The PA signal generated by the bone contains both the microstructural information and molecular information, which are both highly correlated with bone health. Lashkari et al. evaluated the cortical and trabecular bone structure and density variations by using a dual backscattered ultrasound and PA radar system [24, 25]. Furthermore, our group has studied the feasibility of accessing BMD and BMA of the trabecular bone in rat models through using thermal photoacoustic (TPA) and photoacoustic spectral analysis (PASA). Recently, Idan Steinberg et al. used the dual-modality multispectral photoacoustic system to quantify the blood/fat ratio present in the marrow, which has been correlated with molecular changes in the long bone.
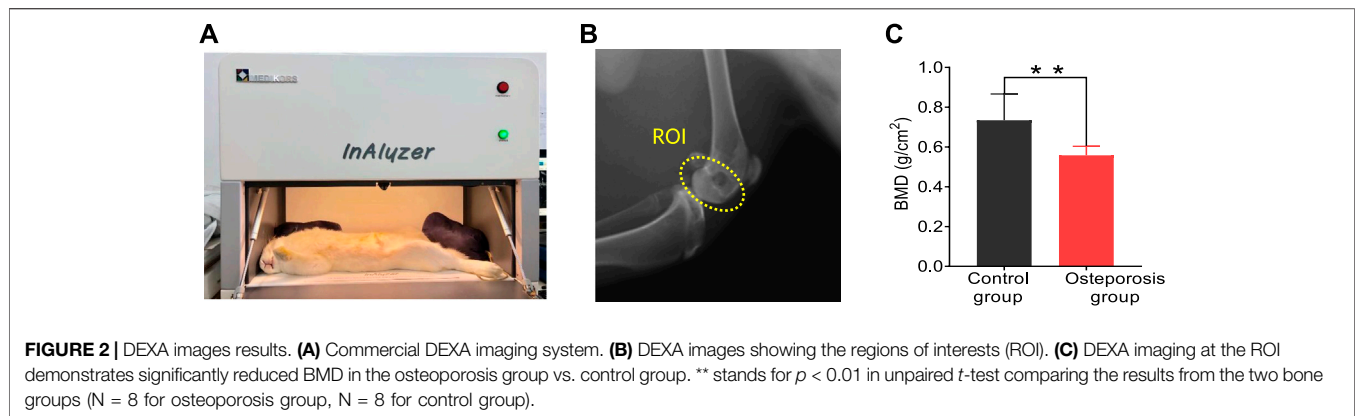
In this study, the feasibility of the multi-wavelength PA analysis (MWPA) technique in quantifying the molecular information of trabecular bone based on rabbit models with different BMDs were studied. The experimental measurements on the rabbit models of control and osteoporosis groups were performed. The PA spectroscopic curves of the bone from different groups were obtained and decomposed. Then, the MWPA parameter "relative composition ratio" of different chemical components including hydroxyapatite, lipid, hemoglobin, oxy-hemoglobin, and whole blood were quantified and compared with the gold-standard X-ray images and the relative optical absorption spectrum obtained by the commercial spectrometer system.

MATERIALS AND METHODS

Experiment Setup

The bone composition of the two groups was measured by using MWPA at the range of 690–950 nm at 10 nm intervals. The experimental setup for studying the chemical components in bone is shown in **Figure 1A**. The light beam generated by an Nd: YAG laser pumped OPO (Vibrant B, Opotek) was divided into two parts. 10% of the laser energy was projected to a black rubber by a beam splitter and recorded by the ultrasound transducer (V310-SU, Olympus) for the calibration of subsequent signal magnitude. The remaining 90% illuminated the bone from one side on the surface of the bone. The diameter of the beam was 4 mm and the light fluency was controlled at 15–20 mJ/cm^2. Light passed through the bone and then excited PA signal. The PA signal was received by a needle hydrophone (HNC-1500, Onda Co., Sunnyvale, CA, United States) with a broad bandwidth from 0 to 10 MHz. A pre-amplifier was connected after the hydrophone to improve the signal-to-noise ratio (SNR), and then it was digitized and recorded by a digital oscilloscope (HDO6000, oscilloscope, Teledyne Lecroy, United States). To enhance the signal-to-noise ratio (SNR), the PA signal was averaged over 50 laser pulses. Furthermore, the gold-standard DEXA images was conducted by the commercial DEXA imaging system (InAlyzer) and the relative optical absorption spectrum obtained by the commercial spectrometer system were conducted for each bone samples.

FIGURE 2 | DEXA images results. **(A)** Commercial DEXA imaging system. **(B)** DEXA images showing the regions of interests (ROI). **(C)** DEXA imaging at the ROI demonstrates significantly reduced BMD in the osteoporosis group vs. control group. ** stands for $p < 0.01$ in unpaired t-test comparing the results from the two bone groups (N = 8 for osteoporosis group, N = 8 for control group).

Animal Models

In this study, the animal bone models we used in the MWPA measurements were distal end of forelimb, as shown in **Figure 1C**. 8 five-month-old, skeletally mature, female New Zealand white rabbits were divided randomly into two groups: osteoporosis group and control group. Bilateral ovariectomy was used in the osteoporosis group to simulate the symptoms of osteoporosis in elderly women, and sham surgery was used in the control group to avoid other factors affecting the experimental results. Twenty weeks after surgery, rabbits were euthanized, and the distal end of forelimb were dissected and subject to PA assessment.

Signal Processing

First, the PA signal received by the Onda hydrophone was calibrated with the PA signal amplitude generated by the black rubber. The signal was related to the laser power of each wavelength. Secondly, the PA signal was transmitted to the frequency domain via fast Fourier transform, and the intensity of the PA frequency power at 0.2–5 MHz was summarized as the PA absorption value of each wavelength without being affected by low frequency (<0.2 MHz) noise or high frequency (>5 MHz) noise. The PA signal of each wavelength of light was then quantified and a PA absorption curve was obtained, which represented the spectral PA absorption of each bone. Thirdly, each bone sample was tested from three different directions in order to reduce measurement errors. The PA spectrum curves were obtained in at three different locations as shown in **Figure 1C** and were averaged for further analysis. Finally, spectral unmixing based on the least-square regression method was conducted, the PA absorption spectrum of each group of bones was decomposed to obtain the proportion of corresponding chemical components.

RESULTS

DEXA Imaging

The DEXA imaging results from osteoporosis group and control group are shown in **Figure 2**. DEXA images showing the regions of interests (ROI) is marked by the yellow circle as shown in **Figure 2B**. Correlations between the BMD results from DEXA
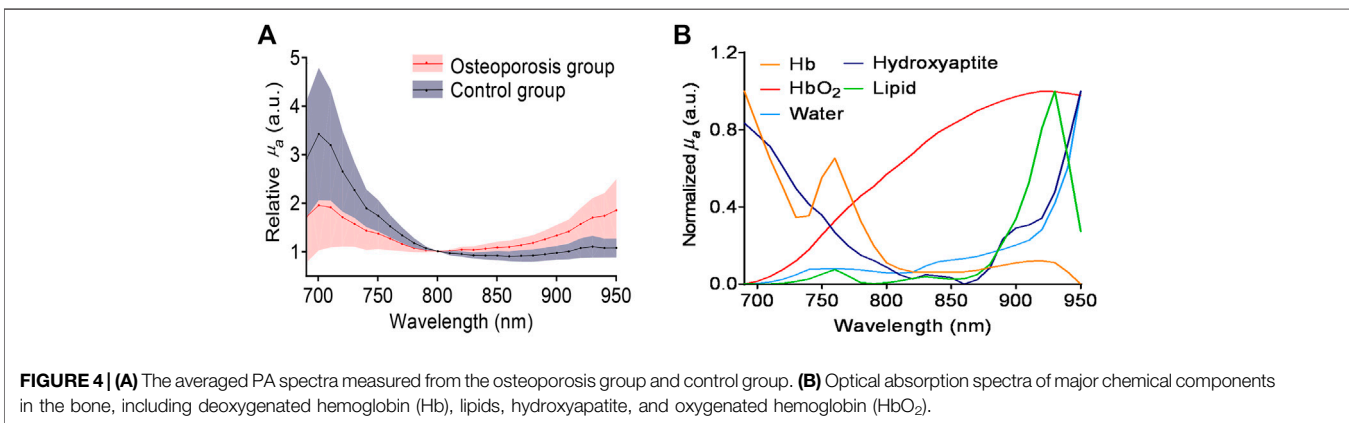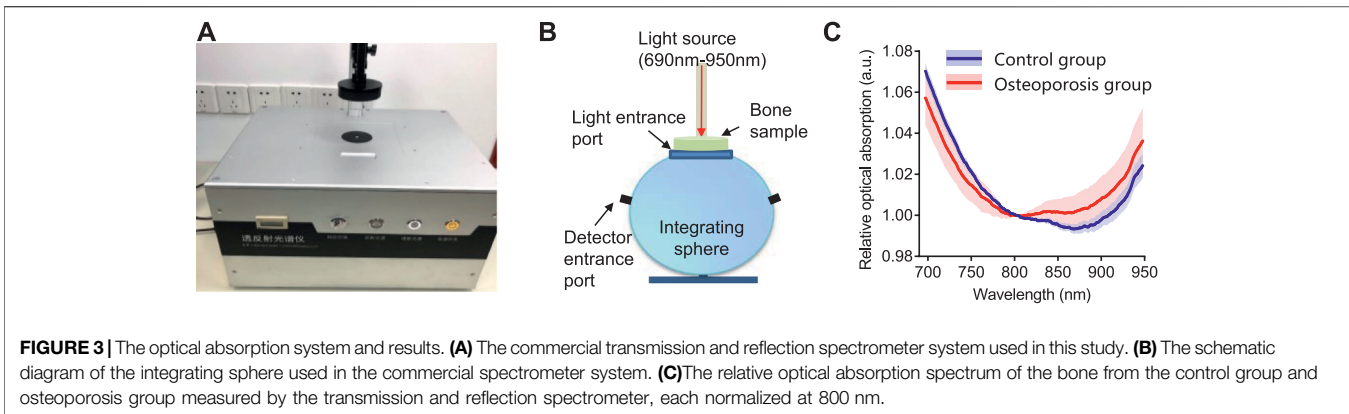
were studied by using unpaired two-tailed independent samples t-tests (with Welch's correction in cases of unequal variances), which lead to $p < 0.01$, as shown in **Figure 2C**. This study based on commercial DEXA technologies confirmed the pathologic conditions of the osteoporosis group as well as the difference between the two groups of rabbit models.

Optical Absorption Measurements

The results of optical absorption measurements are shown in **Figure 3**. **Figures 3AB** shows the commercial spectrometer system and the working principle. The mean and standard deviations of the relative optical absorption spectrum of the bone samples from the osteoporosis group and control group are compared in **Figure 3C**. By comparing with the control group, the bone sample from osteoporosis group has higher optical absorption at the range of 800–950 nm and lower optical absorption at the range of 690–800 nm.

Multi-Wavelength Photoacoustic Measurements

In the spectral range of 690–950 nm, the main optical absorption components in the bone are oxygenated hemoglobin, deoxygenated hemoglobin, mineral (mostly hydroxyapatite), lipid. **Figure 4** shows the MWPA results of the osteoporosis group and control group. The two solid lines in **Figure 4A** show the averaged PA spectra measured from the two groups of bone samples, while the standard deviation is shown by the shaded area next to each curve. It is obviously that the absorption reached its peaks at 700, 760, and 930 nm. The difference is that the absorption of the osteoporosis group near 700–760 nm is stronger than that of the control group, while the absorption of the control group near 930 nm is stronger than that of the osteoporosis group. As expected, the corresponding content of the components in the osteoporosis group and the control group is consistent with the optical absorption results obtained by the commercial spectrometer system shown in **Figure 3C**. The optical absorption spectra of the main chemical components in the bone are shown in **Figure 4B**. By comparing the wavelength positions of the PA signal peaks and the component absorption peaks, it can be found that the strong absorption peak at 700 nm is mainly caused by the absorption of

FIGURE 3 | The optical absorption system and results. **(A)** The commercial transmission and reflection spectrometer system used in this study. **(B)** The schematic diagram of the integrating sphere used in the commercial spectrometer system. **(C)** The relative optical absorption spectrum of the bone from the control group and osteoporosis group measured by the transmission and reflection spectrometer, each normalized at 800 nm.

FIGURE 4 | (A) The averaged PA spectra measured from the osteoporosis group and control group. **(B)** Optical absorption spectra of major chemical components in the bone, including deoxygenated hemoglobin (Hb), lipids, hydroxyapatite, and oxygenated hemoglobin (HbO₂).
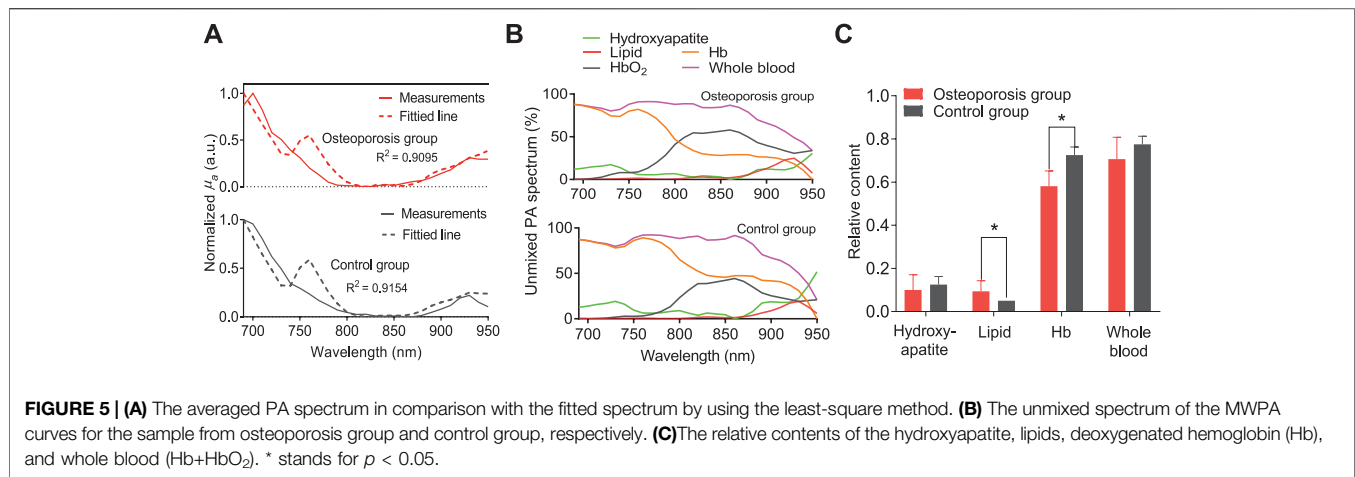
deoxygenated hemoglobin and hydroxyapatite. The absorption peak at 930 nm is mainly contributed by the lipid. Therefore, it can be preliminarily estimated that the lipid content of the osteoporosis group is higher than that of the control group, which is consistent with the past study [1, 9]. Besides, the deoxygenated hemoglobin content and the hydroxyapatite content are lower than that of the control group in the animal bone models we used.

For the PA absorption spectrum for each bone sample, it is given as [26]

$$[\mu_a(\lambda)]_{bone} = \sum_{i=1}^{n} [\mu_a(\lambda)]_i \cdot c_i \qquad (1)$$

Where $\mu_a(\lambda)$ is the PA absorption spectrum as shown in **Figure 4A**, n is the number of chromophore (absorber) types and c_i and $\mu_a(\lambda)$ are the concentration and absorption coefficient of i th chromophore type, respectively. The goal of quantitative WMPA unmixing is to estimate the relative concentration of a particular chemical component from the measurements given the known absorption spectrum $(\mu_a)_i$ of different chemical component. Thus, with the optical absorption spectra $[\mu_a(\lambda)]_i$ of the major chemical components in the bone known [27, 28], the relative content of each chemical component c_i to the PA absorption spectrum can be derived by performing a spectral

unmixing. The spectral unmixing based on the least-square regression method was adopted to obtain the quantitative changes in the contents of the chemical components [29]. **Figure 5A** shows the PA spectrum and the fitted spectrum of the osteoporosis group and the control group, respectively. The R^2 of the osteoporosis group and control was as high as 0.9095 and 0.9154, respectively. After the spectral unmixing, the relative contents of the five chemical components in the bone, including deoxygenated hemoglobin, lipid, hydroxyapatite, and oxygenated hemoglobin, were derived. The results of the two groups of bone samples are shown in **Figure 5B**. To evaluate whether each of the differences in chemical properties between the two bone groups has statistical significance, an unpaired two-tailed independent samples t-test (with Welch's correction in cases of unequal variances) was conducted. Compared to the control group, the chemical changes in the osteoporosis group showing statistical significance include the increased lipid content, the decreased deoxy-hemoglobin content which are correlation with the osteoporosis diseases. Compared to the control group, the bones in the osteoporosis group also show decreased hydroxyapatite content, whole blood content, which, however, is not statistically significant. These noticed chemical changes of lipid, hydroxyapatite and whole blood in osteoporosis bones are matched well with the findings reported in previous publications [10, 30–34]. However, for the *ex vivo* bone, the deoxygenated

FIGURE 5 | (A) The averaged PA spectrum in comparison with the fitted spectrum by using the least-square method. **(B)** The unmixed spectrum of the MWPA curves for the sample from osteoporosis group and control group, respectively. **(C)** The relative contents of the hydroxyapatite, lipids, deoxygenated hemoglobin (Hb), and whole blood (Hb+HbO$_2$). * stands for $p < 0.05$.

hemoglobin and oxygenated hemoglobin are different from the *in vivo* bone sample, especially for the oxygenated hemoglobin. For example, the past study demonstrated the deoxygenation of blood in the *ex vivo* specimens and revealed that deoxygenation of blood occurs almost immediately after sacrificing the animals [35]. Therefore, in this *ex vivo* study, we did not compare the content of oxygenated hemoglobin for osteoporosis bone samples and control samples. Besides, since the deoxygenation of blood occurs in the bone samples, the blood was mostly composited by deoxygenated hemoglobin for the *ex vivo* bone samples in this study. It means that the total content of deoxygenated hemoglobin is highly related with the amount of the whole blood in the bone. Due to the fact that the amount of blood in the normal bone sample is higher than that in the osteoporosis bone sample [12], therefore, the deoxygenated hemoglobin in the control group is higher by comparing with the osteoporosis group in this *ex vivo* study.

CONCLUSION AND DISCUSSION

The results of this study indicate the feasibility of MWPA method in assessing bone chemical composition. In addition to measuring the mineral content in bones, it can also measure the content of chemical components such as lipid, oxygenated hemoglobin and deoxygenated hemoglobin. The content and changes of these ingredients are inextricably related to bone health, and has the potential to used as a new way for bone health assessment.

This study currently has some limitations. First, the number of bone samples is not large enough. There are only four rabbit samples in each group, and only eight sets of data can be obtained, so data analysis is not universal. In the future, additional data should be collected and analyzed on a large group of samples. Second, the chemical composition has not been verified using the bone histomorphometry. In the future work, we plan to further indicate the differences in lipid and Hb content of those two groups though other pathways. For example, the MRI imaging can be used to get the lipid fraction as the gold-standard for lipid content [10, 36, 37]. The reticular fiber staining for quantification of blood vessels can be used as the gold-standard to reveal the differences in blood content of those two groups. Third, the influence of different

types of fatty acids as well as the content of collagen which are also related with bone health are not considered in this study. In the future, with the wider range of the laser wavelength and higher resolution of scanning, it has the potential to distinguish the changes in different types of fatty acids and contents of collagen in the bone tissue. Forth, this study is mainly focusing on the isolated bones. In the future, this technology has the potential to be applied for clinical study *in vivo*. For *in vivo* study, the bone assessment technique based on the PA detecting method described in our manuscript may be not available and should be optimized with better design. For example, the transmission PA mode for multi-wavelength PA measurement of bone *in vivo* in our study published recently [38]. In addition, the effects of light attenuation and ultrasound attenuation need to be considered. Besides, not only the bone but also the overlying soft tissue absorb the light and leads to an increase of light attenuation. Therefore, it is necessary to consider the effect of light attenuation in the bone tissue as well as the overlying soft tissue. At the same time, it has a high attenuation of PA signal for the *in vivo* PA measurements, especially for the high frequency components. Thus, the optimized center frequency of the transducer at a relative lower frequency should be used.

Despite these limitations, this study has successfully demonstrated the feasibility of the emerging PA technology in assessing the chemical information in bones. Compared with DEXA, MRI, QUS and light based techniques, MWPA has the potential to provides more comprehensive bone assessment results, including not only the chemical compositions of bone but also the micro-structure which is highly correlated with bone health as reported in our previous paper [39]. For the gold standard DEXA imaging, since the X-rays are attenuated by both bone and bone marrow fat, therefore, the BMD results quantified by DEXA is altered by the changes in the lipid content of bones. For MRI, in particular MRI spectroscopy, it allows the quantification of bone marrow fats, however, it cannot provide the information of BMD [1]. In addition, the QUS cannot be used for assessing the components of bone composition. Besides, compared with the light based techniques, the PA sensing is based on the detection of light-induced ultrasonic signals which are much less scattered in biological tissues, it can present more spatial information in deep tissues than pure optical techniques. Furthermore, the PA bone assessment method proposed in this article has many

advantages such as target-specific, non-ionizing, low-cost, and patient friendly. With all these unique advantages, this technology is expected to be improved and developed into a more accurate bone evaluation method in the future.

DATA AVAILABILITY STATEMENT

The original contributions presented in the study are included in the article/Supplementary Material, further inquiries can be directed to the corresponding author.

ETHICS STATEMENT

The animal study was reviewed and approved by Animal Ethics Committee of Tongji University, Shanghai.

AUTHOR CONTRIBUTIONS

FUNDING

REFERENCES

1. Di Pietro G, Capuani S, Manenti G, Vinicola V, Fusco A, Baldi J, et al. Bone marrow lipid profiles from peripheral skeleton as potential biomarkers for osteoporosis: a 1H-MR spectroscopy study. *Acad Radiol* (2016) 23(3):273–83. doi:10.1016/j.acra.2015.11.009

2. Kanis JA. Diagnosis and clinical aspects of osteoporosis. In: *Pocket reference to osteoporosis*. Dordrecht, Netherlands: Springer (2019). p 11–20.

3. Marcocci C, Saponaro F. *Osteoporosis diagnosis, multidisciplinary approach to osteoporosis*. Dordrecht, Netherlands: Springer (2018). p 45–57.

4. Raum K, Leguerney I, Chandelier F, Bossy E, Talmant M, Saïed A, et al. Bone microstructure and elastic tissue properties are reflected in QUS axial transmission measurements. *Ultrasound Med Biol* (2005) 31(9): 1225–35.doi:10.1016/j.ultrasmedbio.2005.05.002

5. Laugier P. Quantitative ultrasound instrumentation for bone in vivo characterization. In: P. Laugier G. Haïat, editors *Bone quantitative ultrasound*. Dordrecht, Netherlands: Springer (2011). p 47–71.

6. Töyräs J, Nieminen M, Kröger H, Jurvelin J. Bone mineral density, ultrasound velocity, and broadband attenuation predict mechanical properties of trabecular bone differently. *Bone* (2002) 31(4):503–7. doi:10.1016/s8756-3282(02)00843-8

7. Liu C, Ta D, Fujita F, Hachiken T, Matsukawa M, Mizuno K, et al. The relationship between ultrasonic backscatter and trabecular anisotropic microstructure in cancellous bone. *J Appl Phys* (2014) 115(6):064906. doi:10.1063/1.4865173

8. Njeh C, Boivin C, Langton C. The role of ultrasound in the assessment of osteoporosis: a review. *Osteoporos Int* (1997) 7(1):7–22. doi:10.1007/BF01623454

9. Griffith JF, Yeung DK, Antonio GE, Lee FK, Hong AW, Wong SY, et al. Vertebral bone mineral density, marrow perfusion, and fat content in healthy men and men with osteoporosis: dynamic contrast-enhanced MR imaging and MR spectroscopy. *Radiology* (2005) 236(3):945–51. doi:10.1148/radiol.2363041425

10. Griffith JF, Yeung DK, Antonio GE, Wong SY, Kwok TC, Woo J, et al. Vertebral marrow fat content and diffusion and perfusion indexes in women with varying bone density: MR evaluation. *Radiology* (2006) 241(3):831–8. doi:10.1148/radiol.2413051858

11. Patsch JM, Burghardt AJ, Kazakia G, Majumdar S. Noninvasive imaging of bone microarchitecture. *Ann N Y Acad Sci* (2011) 1240:77–87. doi:10.1111/j.1749-6632.2011.06282.x

12. Pifferi A, Torricelli A, Taroni P, Bassi AL, Chikoidze E, Giambattistelli E, et al. Optical biopsy of bone tissue: a step toward the diagnosis of bone pathologies. *J Biomed Optic* (2004) 9(3):474–80. doi:10.1117/1.1691029

13. Schulmerich MV, Dooley K, Morris MD, Vanasse TM, Goldstein SA. Transcutaneous fiber optic Raman spectroscopy of bone using annular illumination and a circular array of collection fibers. *J Biomed Optic* (2006) 11(6):060502. doi:10.1117/1.2400233

14. Morris MD, Mandair GS. Raman assessment of bone quality. *Clin Orthop Relat Res* (2011) 469(8):2160–9. doi:10.1007/s11999-010-1692-y

15. Draper ER, Morris MD, Camacho NP, Matousek P, Towrie M, Parker AW, et al. Novel assessment of bone using time-resolved transcutaneous Raman spectroscopy. *J Bone Miner Res* (2005) 20(11):1968–72. doi:10.1359/JBMR.050710

16. Ailavajhala R, Oswald J, Rajapakse CS, Pleshko N. Environmentally-controlled near infrared spectroscopic imaging of bone water. *Sci Rep* (2019) 9(1):10199. doi:10.1038/s41598-019-45897-3

17. Paschalis E, Gamsjaeger S, Klaushofer K. Vibrational spectroscopic techniques to assess bone quality. *Osteoporos Int* (2017) 28(8):2275–91. doi:10.1007/s00198-017-4019-y

18. Mandair GS, Steenhuis P, Ignelzi MA, Morris MD. Bone quality assessment of osteogenic cell cultures by Raman microscopy. *J Raman Spectrosc* (2018) 50(3): 360–70. doi:10.1002/jrs.5521

19. Wang X, Pang Y, Ku G, Xie X, Stoica G, Wang LV. Noninvasive laser-induced photoacoustic tomography for structural and functional *in vivo* imaging of the brain. *Nat Biotechnol* (2003) 21(7):803–6. doi:10.1038/nbt839

20. Wang LV, Hu S. Photoacoustic tomography: in vivo imaging from organelles to organs. *Science* (2012) 335(6075):1458–62. doi:10.1126/science.1216210

21. Steinberg I, Huland DM, Vermesh O, Frostig HE, Tummers WS, et al.. Photoacoustic clinical imaging. *Photoacoustics* (2019) 14:77–98. doi:10.1016/j.pacs.2019.05.001

22. Zhang W, Oraiqat I, Lei H, Carson PL, EI Naqa I, Wang X. Dual-modality X-ray-induced radiation acoustic and ultrasound imaging for real-time monitoring of radiotherapy. *BME Front* (2020) 2020:9853609. doi:10.34133/2020/9853609

23. Zhu Y, Lu X, Dong X, Yuan J, Fabiilli ML, Wang X. LED-based photoacoustic imaging for monitoring angiogenesis in fibrin scaffolds. *Tissue Eng C Methods* (2019) 25(9):523–31. doi:10.1089/ten.TEC.2019.0151

24. Lashkari B, Yang L, Mandelis A. The application of backscattered ultrasound and photoacoustic signals for assessment of bone collagen and mineral contents. *Quant Imaging Med Surg* (2015) 5(1):46–56. doi:10.3978/j.issn.2223-4292.2014.11.11

25. Yang L, Lashkari B, Mandelis A, Tan JW. Bone composition diagnostics: photoacoustics versus ultrasound. *Int J Thermophys* (2015) 36(5–6):862–7. doi:10.1007/s10765-014-1701-6

26. Kim MW, Jeng GS, O'Donnell M, Pelivanov I. Correction of wavelength-dependent laser fluence in swept-beam spectroscopic photoacoustic imaging with a hand-held probe. *Photoacoustics* (2020) 19:100192. doi:10.1016/j.pacs.2020.100192

27. Jacques SL. Optical properties of biological tissues: a review. *Phys Med Biol* (2013) 58(11):R37. doi:10.1088/0031-9155/58/11/R37

28. Feng T, Kozloff KM, Tian C, Perosky JE, Hsiao Y-S, Du S, et al. Bone assessment via thermal photo-acoustic measurements. *Opt Lett* (2015) 40(8):1721–4. doi:10.1364/OL.40.001721

29. Udelhoven T, Emmerling C, Jarmer T. Quantitative analysis of soil chemical properties with diffuse reflectance spectrometry and partial least-square regression: a feasibility study. *Plant Soil* (2003) 251(2):319–29. doi:10.1023/A:1023008322682

30. Patsch JM, Li X, Baum T, Yap SP, Karampinos DC, Schwartz AV, et al.. Bone marrow fat composition as a novel imaging biomarker in postmenopausal women with prevalent fragility fractures. *J Bone Miner Res* (2013) 28(8): 1721–8. doi:10.1002/jbmr.1950

31. Oei L, Koromani F, Rivadeneira F, Zillikens MC, Oei EH. Quantitative imaging methods in osteoporosis. *Quant Imaging Med Surg* (2016) 6(6):680–98. doi:10.21037/qims.2016.12.13

32. Rubin MR, Patsch JM. Assessment of bone turnover and bone quality in type 2 diabetic bone disease: current concepts and future directions. *Bone Res* (2016) 4:16001. doi:10.1038/boneres.2016.1

33. Shen W, Scherzer R, Gantz M, Chen J, Punyanitya M, Lewis CE, et al. Relationship between MRI-measured bone marrow adipose tissue and hip and spine bone mineral density in African-American and Caucasian participants: the CARDIA study. *J Clin Endocrinol Metab* (2012) 97(4): 1337–46. doi:10.1210/jc.2011-2605

34. Bredella MA, Daley SM, Kalra MK, Brown JK, Miller KK, Torriani M. Marrow adipose tissue quantification of the lumbar spine by using dual-energy CT and single-Voxel (1)H MR spectroscopy: a feasibility study. *Radiology* (2015) 277(1):230–5. doi:10.1148/radiol.2015142876

35. Salomatina E, Yaroslavsky A. Evaluation of the *in vivo* and *ex vivo* optical properties in a mouse ear model. *Phys Med Biol* (2008) 53(11):2797–807. doi:10.1088/0031-9155/53/11/003

36. Patsch JM, Li X, Baum T, Yap SP, Karampinos DC, Schwartz AV, et al. Bone marrow fat composition as a novel imaging biomarker in postmenopausal women with prevalent fragility fractures. *J Bone Miner Res* (2013) 28(8):1721–8. doi:10.1002/jbmr.1950

37. Baofeng L, Zhi Y, Bei C, Guolin M, Qingshui Y, Jian L. Characterization of a rabbit osteoporosis model induced by ovariectomy and glucocorticoid. *Acta Orthop* (2010) 81(3):396–401. doi:10.3109/17453674.2010.483986

38. Feng T, Zhu Y, Wang X. Functional photoacoustic and ultrasonic assessment of osteoporosis–a clinical feasibility study. *BME Front* (2020) 2020:1081540. doi:10.34133/2020/1081540

39. Feng T, Perosky JE, Kozloff KM, Xu G, Cheng Q, Du S, et al. Characterization of bone microstructure using photoacoustic spectrum analysis. *Opt Express* (2015) 23(19):25217–24. doi:10.1364/OE.23.025217

Conflict of Interest: The authors declare that the research was conducted in the absence of any commercial or financial relationships that could be construed as a potential conflict of interest.